第35卷第10期 焊 接 学 报 Vol. 35 No. 10
2014年10月 TRANSACTIONS OF THE CHINA WELDING INSTITUTION October 2014

TA15钛合金激光非晶－纳米晶增强镍基涂层的组织结构及耐磨性

李嘉宁[1,2]， 巩水利[1]， 李怀学[1]， 单飞虎[1]
(1. 北京航空制造工程研究所 高能束流加工技术重点实验室，北京 100024;
2. 中航工业北京航空材料研究院，北京 100095)

摘 要：在重要航空材料TA15钛合金基材表面进行激光同轴送粉熔覆Ni60A-Ni包$WC-TiB_2-Y_2O_3$混合粉末可生成非晶－纳米晶增强复合涂层. 对涂层进行微观组织观察、显微硬度测试及室温干摩擦磨损试验. 结果表明，涂层主要由γ-(Fe，Ni)，WC，α-W_2C，$M_{12}C$，Ti-B化合物，Ti-Al金属间化合物，Mo，Zr与V元素的碳化物以及非晶相构成. 整个涂层为非晶、纳米晶及其它晶化相共存. 涂层较TA15钛合金表现出更好的耐磨损性，且涂层的主要磨损机制为磨粒磨损与粘着磨损. 纳米晶颗粒的产生可使涂层磨损表面光滑，有利于摩擦系数与磨损量的降低.

关键词：激光熔覆；表面改性；磨损性能
中图分类号：TG 159.9 **文献标识码**：A **文章编号**：0253－360X(2014)10－0057－04

0 序 言

TA15钛合金属于高铝当量损伤容限型钛合金，是中国航空工业中重要的结构材料之一，但其耐磨性较差，一定程度上限制了其应用范围. 激光熔覆是一种新型的表面改性技术，可以针对航空材料不同的服役条件，利用高能密度激光束加热冷却速度快等特点，在结构件表面制备非晶－纳米晶增强金属陶瓷复合涂层，从而达到航空材料表面改性的目的[1,2].

近年来，随着纳米材料和纳米技术的飞速发展，纳米相关技术开始被应用于表面工程，于是形成了“纳米表面工程”的新领域，长期以来一直作为一个特殊的应用领域受到国内外军方的高度重视[3]. 非晶态合金兼有一般金属与玻璃的特性，因而具有独特的物理化学与力学性能，如极高的强度、韧性、抗磨损及耐蚀性[4－6]. 将纳米晶与非晶同时应用于航空材料表面的激光熔覆涂层中将极大提高航空材料的表面性能. 文中提出将Ni60A-Ni包$WC-TiB_2-Y_2O_3$混合粉末激光熔覆于TA15基材表面从而改善基材的耐磨损性能. 试验表明，通过该方法可在TA15基材表面形成具有极强耐磨损性能的非晶－纳米晶增强复合涂层.

收稿日期：2013－02－07
基金项目：国防重大基础科研资助项目；中国博士后科学基金面上资助项目(2012M520135)

文中分析了TA15钛合金表面Ni60A-Ni包$WC-TiB_2-Y_2O_3$激光熔覆涂层的组织结构与摩擦磨损性能，为激光熔覆技术在航空零部件生产与修复领域的应用提供了理论与试验依据.

1 试验方法

试验材料包括基材与熔覆材料两部分. 基材为TA15钛合金，其名义化学成分(质量分数，%)：6.06Al，2.08Mo，1.32V，1.86Zr，0.09Fe，0.08Si，0.05C，0.07O，余量为Ti；熔覆材料：Ni60A(纯度≥99.5%，50目～200目)、Ni包WC(纯度≥99.5%，50目～100目，20 Ni)、TiB_2(纯度≥99.5%，50目～100目)以及Y_2O_3(纯度≥99.5%，10目～50目)，其中Ni60A名义化学成分：0.8C，15Cr，3B，4Si，10Fe，余量为Ni. 熔覆材料成分配比(质量分数，%)：69Ni60A-20Ni包WC-10TiB_2-1Y_2O_3. 钛合金熔覆式样尺寸：10 mm×10 mm×10 mm(微观组织结构分析)与30 mm×10 mm×10 mm(磨损测试).

通过德国通快TRUMPF生产的TLF1500 TURBO快速轴流型激光器采用同轴送粉方式进行激光熔覆，其最大输出功率为15 kW. 激光器和DPSF-3型同轴送粉器对试样表面进行激光熔覆工艺处理，工艺参数：激光功率1 kW，光斑直径4 mm，扫描速度2～7 mm/s，送粉率为15 g/min. 为了避免激光熔覆过程中合金氧化，采用氩气作为保护气体，经过特

制的喷嘴直接吹向试样的熔覆表面，气体流量为 15 L/min，多道搭接率为 35%.

采用 CSM950 型扫描电子显微镜观察涂层的微观组织形貌；采用 Rigaku D/max-rB 型 X 射线衍射仪对涂层进行物相分析；用 JEM-2010 高分辨透射电镜对金属薄膜试样的高倍组织形貌进行观察和电子选区衍射分析；利用 MM-200 型环－块摩擦磨损试验机进行室温干滑动摩擦试验，对磨轮为 20% Co-WC 硬质合金，硬度≥80 HRA. 磨损试验过程中试样固定，磨轮以 400 r/min 的速度转动，线速度为 0.95 m/s.

2 试验结果与分析

2.1 涂层组织结构与显微硬度

图 1 为涂层不同位置的微观组织. 图 1a 表明，激光熔覆涂层与基材之间形成了良好的冶金结合，且有大量片状/棒状/网状的析出物弥散分布于涂层底部. 激光熔覆过程中，大量 Ti，Al，Mo，V，Zr 元素由基材进入熔池. Mo，Zr，V 均属于较强的碳化物形成元素，熔覆过程中其所生成的碳化物稳定且不易长大，质点细小而稳定，可有效地阻止晶界移动，细化涂层组织[7]. 图 1b 为 TA15 基材热影响区的 SEM 形貌，可见热影响区的微观组织类型均为等轴组织，由初生等轴 α 相、较小的次生等轴 α 相、被拉长的初生等轴 α 与 β 转变基体构成，且各组分形态与大小基本相当.

图 1c 表明大量细小的白色颗粒状、长条状析出物弥散分布于涂层熔合区基底之上. 分析可知，白色颗粒状析出物为未完全生长的陶瓷相，长条状析出物为硼化物，而基底的主要组成为金属与奥氏体相. TiB_2 等陶瓷相的加入可显著细化涂层晶界处的网状共晶结构；另外，适量 Y_2O_3 稀土氧化物的添加可提升液态金属的流动性，减小凝固过程中成分过冷，降低成分偏析，减弱枝晶生长方向性，使涂层组织均匀细化[8].

如图 1d 所示，球状陶瓷析出相在涂层中产生. 在熔池冷却初期，未熔解的陶瓷颗粒为非均匀晶核的结晶提供了形核点，促使极为细小的卵状析出相在涂层中形成，利于改善涂层韧性. 图 1e 所示的棒状析出相为涂层中硼化物的 SEM 形貌. 通常硼化物在激光熔覆层中呈现不同的组织结构，如片状、棒状或网状等.

图 1f 表明大量的纳米晶颗粒在涂层基底处发生聚集. 这是由于纳米晶颗粒具有极大的比表面积，易发生聚集形成第二相粒子以降低系统的界面

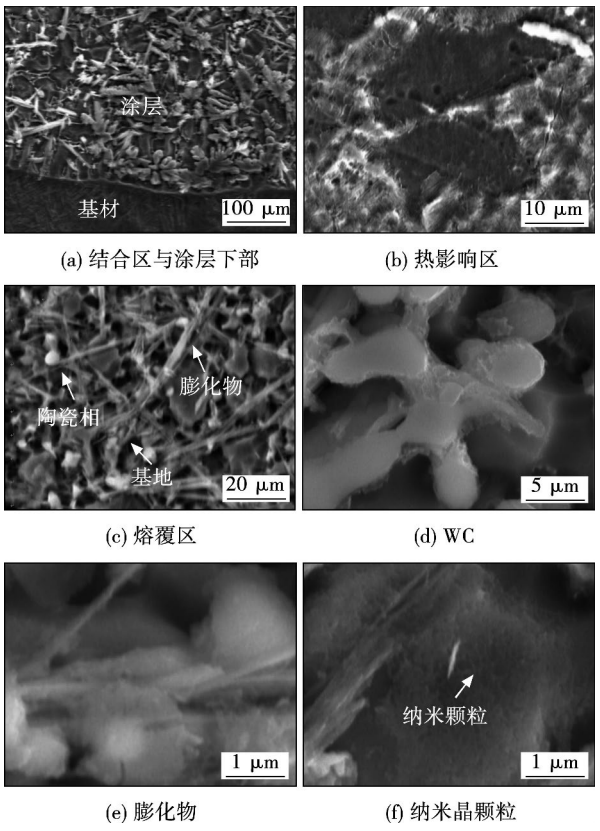

(a) 结合区与涂层下部 (b) 热影响区

(c) 熔覆区 (d) WC

(e) 膨化物 (f) 纳米晶颗粒

图 1 涂层不同位置的微观组织

Fig. 1 Microstructures of different locations of coating

能量；另外，激光熔池具有扩散和对流两种传质形式，熔池在急速凝固过程中，亚稳定相得不到向稳定相转变的激活能而可能保存下来；随着凝固速率的进一步提高，亚稳定相的析出也可能被抑制，已成形的晶核来不及长大熔池就已凝固，从而形成纳米晶相[9].

用透射电镜对由涂层中部取出的薄膜样品进行观察分析(图 2)，其 TEM 图象表明，由于激光熔覆具有加热及冷却速度快的特点，熔体成分在宏观上保持均匀的同时，在微观上却存在着微区内成分不均匀的现象(图 2a). 对箭头所指区域进行电子选区衍射，如图 2b 所示，电子选区衍射图谱呈现为表征非晶相的漫散晕环加纳米晶相的多晶衍射环，按透射电镜的相机常数计算、标定，此晶化相为 TiB_2 多晶体，该多晶体沿(100)，(101)，(002)平面生长.

图 2c 为涂层表层的 X 射线衍射图. 由该图可知，涂层表层主要包括 γ-(Fe，Ni)，Ti-B，WC，α-W_2C 及 $M_{12}C$ 相；另外，根据之前分析可知，涂层所含成分较为复杂，还包含少量的 Ti-Al 金属间化合物以及 Mo、Zr 及 V 元素的碳化物等相. 衍射图还表明宽的漫散衍射峰出现在 2θ 等于 15°～30°，36°～47°以及 70°～80°，且有几个尖锐的晶化衍射峰叠加在漫散衍射峰之上，证明涂层中同时存在非晶相与其它晶

化相. 结果表明，整个涂层为非晶、纳米晶及其它晶化相共存.

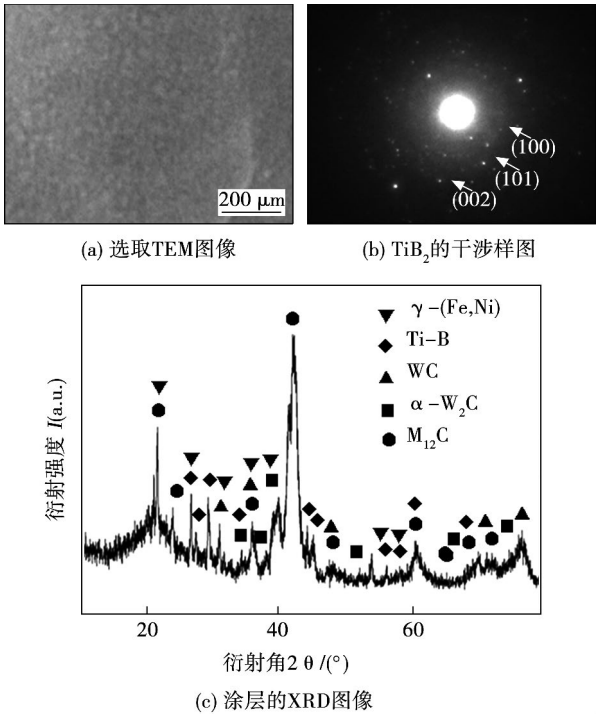

(a) 选取TEM图像　　(b) TiB_2的干涉样图

(c) 涂层的XRD图像

图 2　涂层的 TEM 图像和 XRD 衍射图谱

Fig. 2　TEM and XRD pattern of coating

硬度测试结果表明，涂层的显微硬度范围在 1 250～1 400 MPa，较 TA15 基材（约 390 MPa）提高了约 3.5 倍. 涂层显微硬度的提高主要归因于 WC，TiB_2 等硬质相、细晶强化、固溶强化以及非晶－纳米晶综合作用的结果.

2.2　涂层摩擦磨损特性

2.2.1　摩擦系数与磨损率

图 3a 表明，涂层的摩擦系数明显低于 TA15 合金的摩擦系数，这是由于涂层相比基材具有较高的显微硬度. 随着载荷的增加，涂层的摩擦系数呈明显下降趋势，而 TA15 合金的摩擦系数曲线却一直保持稳定. 此过程中涂层摩擦系数的降低表明在不同载荷作用下，涂层相对基材表现出更好的耐磨性.

图 3b 的磨损试验结果表明，当载荷为 49 N，经 40 min 干滑动摩擦后，涂层的磨损体积约为 TA15 基材的 1/12，表明涂层较 TA15 基材表现出更好的耐磨损性能. 涂层中包含大量颗粒增强相，在此条件下耐磨损性能不仅与涂层硬度有关，还与颗粒增强相的硬度与形态有关. 另外，磨损过程中，纳米晶增强相阻碍涂层基底的塑性形变，有利于涂层耐磨损性能的提高[10]；少量 Y_2O_3 的加入使涂层晶界得到强化，晶粒之间的滑移传递较易，有利于促进磨擦过程中表面微裂纹顶部的应力松弛，增加裂纹的扩展阻力，提高涂层的塑性及力学性能，减轻磨损量.

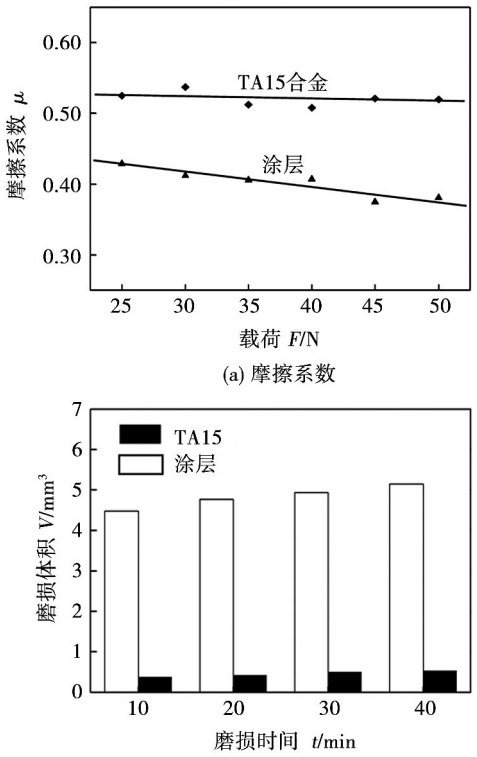

(a) 摩擦系数

(b) 摩损体积

图 3　TA15 合金与涂层的摩擦系数与磨损体积

Fig. 3　Coefficients of friction and wear volume losses of TA15 alloy and coating

2.2.2　摩擦磨损机理

图 4a 为载荷 49 N，经 40 min 干滑动摩擦后，TA15 钛合金的 SEM 磨损形貌. 可推断 TA15 合金的磨损过程为显微切削与粘着损失，呈典型的粘着磨损形貌. 由于 TA15 基材具有塑性好与硬度低的特点，磨损过程中，磨轮表面的硬质点对基材发生显微切削，形成深而长的犁沟.

涂层的磨损形貌则较为光滑平整（图 4b）. 其磨损表面的犁沟尽管存在，但已不明显，摩擦痕迹细而浅，但方向紊乱. 这主要由于涂层的显微硬度较高，磨轮表面微凸起对涂层的犁削作用减弱. 从微观角度分析，纳米颗粒具有极高的强度与硬度，作为硬质相而使涂层得到强化，在与摩擦副对磨的过程中发挥了强烈的阻磨作用[11]；另外，由于非晶－纳米晶的反复塑性变形量小，加之高硬度的纳米晶使裂纹的扩展变的困难，因此涂层表现出良好的耐磨损性能.

图 4c 为涂层磨损表面经过熔液腐蚀后的 SEM 形貌，表明大量纳米颗粒存在于涂层的磨损表面，纳米颗粒的存在可使涂层磨损表面光滑，有利于摩擦

系数与磨损量的降低.

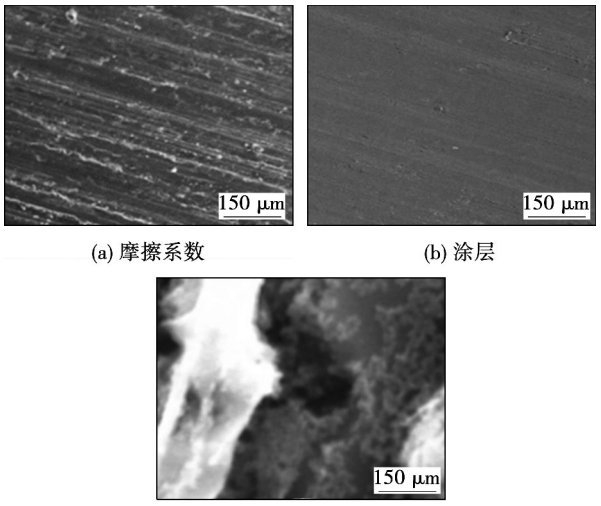

(a) 摩擦系数 (b) 涂层

(c) 腐蚀后的涂层

图 4 涂层与 TA15 合金的磨损形貌

Fig. 4 Worn morphologies of coating and TA15 alloy

3 结 论

(1) 在 TA15 钛合金表面采用同轴送粉方式激光熔覆 Ni60A-Ni 包 $WC-TiB_2-Y_2O_3$ 混合粉末可形成非晶 - 纳米晶增强复合涂层. 涂层主要由 γ-(Fe, Ni), WC, α-W_2C, $M_{12}C$, Ti-B 化合物、Ti-Al 金属间化合物、大量碳化物及非晶相构成.

(2) 大量纳米晶颗粒具有极大的比表面积,易发生聚集形成第二相粒子以降低系统的界面能. 涂层中的晶化相形状、大小各不相同,并与非晶相相间分布;纳米晶相不仅镶嵌于非晶相上,也分布于晶化相之中,整个涂层为非晶、纳米晶及其它晶化相共存.

(3) 涂层的显微硬度较 TA15 基材提高了约 2.5 倍. 涂层在 WC, TiB_2 等硬质相、细晶及非晶 - 纳米晶的综合作用下,较基材显示出更好的耐磨性,涂层的摩擦系数及磨损体积均明显小于基材.

参考文献:

[1] 李 刚, 夏延秋, 王彦芳, 等. 激光熔覆 Zr-Al-Ni-Cu 复合涂层组织及其摩擦磨损性能 [J]. 摩擦学学报, 2002, 22(5): 342 - 346.
Li Gang, Xia Yanqiu, Wang Yanfang, *et al*. Microstructure and tribological properities of laser clad Zr-Al-Ni-Cu composite coating [J]. Tribology, 2002, 22(5): 342 - 346.

[2] 张 松, 周 磊, 郝玉喜, 等. Monel 合金表面激光熔覆镍基合金的组织及摩擦磨损性能 [J]. 焊接学报, 2013, 34(1): 9 - 12.
Zhang Song, Zhou Lei, Hao Yuxi, *et al*. Microstructure and tribological performance of laser clad Ni-base alloy on Monel alloy [J]. Transactions of the China Welding Institution, 2013, 34(1): 9 - 12.

[3] 王 铀. 大力发展纳米表面工程 [J]. 热喷涂技术. 2011, 3(1): 8 - 16.
Wang You. To develop nano-surface engineering [J]. Thermal Spray Technology, 2011, 3(1): 8 - 16.

[4] Zhu Y Y, Huang J, Li Z G, *et al*. Microstructures and properties of Fe-Co-B-Si-Nb coating prepared by laser cladding and remelting [J]. China Welding, 2011, 20(1): 54 - 58.

[5] 张培磊, 李铸国, 姚成武, 等. 激光制备 Fe-Ni 基非晶复合涂层退火性能分析 [J]. 焊接学报, 2011, 32(4): 13 - 16.
Zhang Peilei, Li Zhuguo, Yao Chengwu, *et al*. Fe-Ni-based amorphous coatings fabricated by laser and annealing performance [J]. Transactions of the China Welding Institution, 2011, 32(4): 13 - 16.

[6] 朱庆军, 邹增大, 王新洪. 稀土 RE 对激光熔覆 Fe 基非晶复合涂层的影响 [J]. 焊接学报, 2008, 29(2): 57 - 60.
Zhu Qingjun, Zou Zengda, Wang Xinhong, *et al*. Influence of rare earths on Fe-based amorphous composite coatings by laser cladding [J]. Transactions of the China Welding Institution, 2008, 29(2): 57 - 60.

[7] 戴起勋. 金属材料学 [M]. 北京: 化学工业出版社, 2005.

[8] Li J N, Gong S L, Chen C Z, *et al*. Physical properties and formation of mechanism of copper/glass modifeid laser nanocrystals-amorphous reinforced coatings [J]. Journal of Physical Chemistry C, 2013, 117(9): 4568 - 4573.

[9] Li J N, Gong S L, Li H X, *et al*. Physical properties and microstructures of Fe_3Al matrix laser amorphous-nanocrystals reinforced coating [J]. Materials Letters, 2013, 92: 235 - 238.

[10] 张永振. 材料的干摩擦学 [M]. 北京: 科学出版社, 2007.

[11] Walker J C, Saranu S R, Kean A H, *et al*. Fe nano-particle coatings for high temperature wear resistance [J]. Wear, 2013, 271(9/10): 2067 - 2079.

作者简介: 李嘉宁, 男, 1982 年出生, 博士. 主要从事激光快速成形及激光表面强化方面的科研工作. 发表论文 30 余篇, 申请专利 6 项. Email: jn2369@163.com

通讯作者: 巩水利, 男, 博士, 研究员, 博士研究生导师. Email: gongshuili@sina.com

Microstructure and wear resistance of laser amorphous-nanocrystals reinforced Ni-based coating on TA15 titanium alloy LI Jianing[1,2], GONG Shuili[1], LI Huaixue[1], SHAN Feihu[1] (1. Science and Technology on Power Beam Processes Laboratory, Beijing Aeronautical Manufacturing Technology Research Institute, Beijing 100024, China; 2. Aviation Industry Corporation of China, Beijing Institute of Aeronautical Materials, Beijing 100095, China). pp 57 - 60

Abstract: Coaxial powder feeding laser cladding of the Ni60A-Ni coated WC-TiB_2-Y_2O_3 mixed powders on the aviation material TA15 titanium alloy substrate can form an amorphous-nanocrystals reinforced composite coating. Such coating was researched by means of the microstructure observation, the microhardness test and the dry friction and wear test at room temperature. Investigation indicated that the such coating mainly consisted of γ-(Fe, Ni), WC, α-W_2C, $M_{12}C$, Ti-B compounds, Ti-Al intermetallics, amorphous phases and the Mo, Zr, V carbides. Amorphous, nanocrystalline and the other crystalline phases were existence in such coating. This coating also exhibited a better wear resistance than TA15 titanium alloy, and abrasive grain wear mechanism and the adhere wear mechanism did the process at the same time during the dry sliding wear process. The productions of the nanocrystals made the worn surface more smooth, favoring the decrease of the coefficient of friction and the wear volume losses.

Key words: laser cladding; surface modifications; wear properties

Weld defect detection by X-ray images method based on Fourier fitting surface LI Xueqin[1], LIU Peiyong[2], YIN Guofu[2], JIANG Honghai[3] (1. School of Mechanical Engineering and Automation, Xihua University, Chengdu 610039, China; 2. School of Manufacturing Science and Engineering, Sichuan University, Chengdu 610065, China; 3. School of Electrical and Mechanical Engineering, Kunming University of Science and Technology, Kunming 650504, China). pp 61 - 64

Abstract: To solve such problems as the strong noise, low contrast and complex background of X-ray image in the weld defect detection, a method of the noise reduction, weld edge segmentation and defects extraction was proposed. The fast discrete curvelet transform and cycle shift were applied to reduce noise of the weld image, and the Otsu method was utilized to extract the weld region by the column gray curves of the image. Cubic Fourier curve was used to fit the column gray curves after preprocessing of weld image, and the adaptive threshold surface was constructed by extending fitting curves to 3D space. Finally, the background and the defect area were segmented accurately with the gray differences of 3D gray image between the original image and the reconstructed surface. Experiment results show that the method can extract weld defects accurately. Compared with traditional defect detection algorithm, it has the lower undetected rate and fewer misinterpretations, the accuracy rate could reach 95%.

Key words: X-ray; weld image; defect detection; curvelet transform; Fourier fitting

Effects of laser scanning welding process on porosity rate of aluminum alloy ZHOU Litao, WANG Wei, WANG Xuyou, WANG Shiyang, SUN Qian (Harbin Welding Institute, China Academy of Machinery Science and Technology, Harbin 150028, China). pp 65 - 68, 72

Abstract: Research of 6061 aluminum alloy was done by using laser-scanning welding. The effects of such scanning parameters as track, width and frequency on porosity tendency were studied. The result showed that laser-scanning welding with the path of vertical, parallel and circular to welds can reduce the porosity of aluminum alloy compared with laser welding without scanning and the circular pattern was the best. The scanning width and scanning frequency of laser also have important influence on porosity, which can be controlled within 0.5% as the scanning width was greater than 0.65 mm and scanning frequency was from 100 to 220 Hz. The producing of porosity was associated with weld shape and the lower of depth-to-width ratio of the weld can help to control the porosity.

Key words: aluminum alloy; laser scanning welding; porosity inhibition

Corrosion behavior of weld joints of substation grounding grid FENG Lajun[1], DENG Bo[1], YAN Aijun[2], ZHANG Jing[1] (1. Material Corrosion and Protection Key Laboratory of Xi'an, Xi'an University of Technology, Xi'an 710048, China; 2. Shaanxi Electric Power Research Institute, Xi'an 710054, China). pp 69 - 72

Abstract: To provide foundation for corrosion protection of the weld metal using in grounding grid, the corrosion difference between the weld and base metal of grounding grid was studied by electrochemical noise and field coupon method. The results showd that there were many transients in the time series of the weld of Q235 steel for grounding grid in soil of Shaanxi Xiaoyi substation, while a few transients in the time series of the Q235 base metal, which indicated that weld corrosion was more sensitive to discharge voltage of grounding grid. The noise resistance of the weld metal, Rn, was 3.38×10^4 Ω/cm^2 during the corrosion process, and the Rn of the weld was 1.44×10^4 Ω/cm^2. The corrosion rate of the weld metal was 0.067 mm/a, and for the welded joint was 0.077 mm/a. The based metal was in a uniform type of corrosion and the weld was mainly in a pitting type of corrosion.

Key words: grounding grid; weld corrosion; electrochemical noise; localized corrosion

Research on toughness weak points of joints of NiCrMoV refractory steel for manufacturing steam turbine rotor LI Yifei[1], CAI Zhipeng[1], PAN Jiluan[1], LIU Xia[1,2], WANG Peng[2], HUO Xin[2], SHEN Hongwei[2] (1. Department of Mechanical Engineering, Tsinghua University, Beijing 100084, China; 2. Shanghai Electric Power Generation Equipment Co. Ltd., Shanghai 200240, China). pp 73 - 76, 80

Abstract: The toughness weak points of multi-layer and multi-pass weld of 30Cr2Ni4MoV refractory steel steam turbine welded rotor were studied by means of simulated heat welded layers with the emphasis on the forming of the toughness weak points and its influence on the toughness. The methods of optical microscope analysis, scanning electron microscopy analysis and transmission electron microscope analysis were utilized. The experimental results show that there are many M-A constituents in the carbon-rich areas of welded layers, which is disadvantageous to the toughness. The influence of the M-A constituents on the weld